ELSEVIER

Journal of Alloys and Compounds 432 (2007) 333–337

Journal of ALLOYS AND COMPOUNDS

www.elsevier.com/locate/jallcom

Catalytic combustion of methane over Mn-substituted Ba-La-hexaaluminate nanoparticles

Shunqing Li [a,b], Xiaolai Wang [a,*]

[a] *State Key Laboratory for Oxo Synthesis and Selective Oxidation, Lanzhou Institute of Chemical Physics, Chinese Academy of Sciences, Lanzhou 730000, PR China*

[b] *The Graduate University of the Chinese Academy of Sciences, Beijing 10039, PR China*

Received 31 March 2006; received in revised form 31 May 2006; accepted 6 June 2006

Available online 24 July 2006

Abstract

Mn-substituted Ba-La-hexaaluminate rod-like nanoparticles with high surface area in the range between 45 and 73 m^2/g have been prepared using the alumina sol as the $(NH_4)_2CO_3$ co-precipitation precursor and the supercritical drying (SCD) method. The properties and microstructures of the catalysts are determined by the ion mobility at high calcination temperature. The nature of the large cation in the mirror plane can affect the Mn^{2+}/Mn^{3+} redox process. The $Ba_{0.2}La_{0.8}MnAl_{11}O_{19-\alpha}$ catalyst possesses the highest catalytic activity owing to the excellent performance of activating oxygen.

Keywords: Ba-La-hexaaluminate; Catalytic combustion; Methane; Nanoparticle

1. Introduction

Hexaaluminate materials are of interest as combustion catalysts for gas turbine applications, due to the high thermal stability associated with their peculiar layered structure that consists of γ-Al_2O_3 spinel block intercalated by planes (mirror planes) in which the largest cations are located [1–4]. Large cations play an important role in the catalytic activity and thermal stability. Several compositions have been investigated [5–7]. The $Ba_{1-x}La_xMnAl_{11}O_{19-\alpha}$ system has received much attention since it possesses the larger cations, which would probably lead to a higher thermal stability [5,8]. Further improvement of the performance of the catalysts is necessary.

Catalytic studies indicate the high activity of hexaaluminate catalyst can be attributed to its high surface area available at the elevated reaction temperatures. The pore structure of the oxide is found to be an important parameter in the catalytic combustion. Microporous catalysts appear to be less active than mesoporous ones, perhaps due to mass transfer limitations at high flow velocities needed for flame stabilization [9]. Since Zarur et al. [10,11] prepared hexaaluminate nanoparticles with high catalytic activities by adopting reverse microemulsion-mediated synthesis method, many efforts have been made to increase the catalytic activity and improve the thermal stability of the catalyst simultaneously [12,13]. We attempt to develop a practical and cost-effective synthesis method to prepare catalysts with high surface areas. Hexaaluminate-based catalysts have been prepared using alumina sol [14] as the $(NH_4)_2CO_3$ co-precipitation precursor and a supercritical drying (SCD) method [15].

In this report, $Ba_{1-x}La_xMnAl_{11}O_{19-\alpha}$ ($x = 1$, 0.8, 0.6, 0.4, 0.2, 0) catalysts were prepared and the catalytic activities for methane combustion were investigated. Moreover, N_2-adsorption, X-ray diffraction (XRD), TEM, diffuse reflectance spectroscopy (DRS), temperature-programmed reduction (TPR) of hydrogen and temperature-programmed desorption (TPD) of oxygen were used to study their structural and morphological properties.

2. Experimental

2.1. Preparation of the catalysts [15,16]

A mixture of appropriate amounts of manganese, lanthanum, barium nitrates with alumina sol solution was poured into a well-stirred container with an

* Corresponding author. Tel.: +86 931 8275727; fax: +86 931 8277787.
E-mail address: lishunqing2003@yahoo.com.cn (X. Wang).

0925-8388/$ – see front matter © 2006 Elsevier B.V. All rights reserved.
doi:10.1016/j.jallcom.2006.06.022

ammonium carbonate solution at 60 °C to form the hexaaluminate precursor precipitate. The slurry was aged for 10 h at 60 °C, and then filtered, washed with distilled water. The filter cake was then dried under supercritical conditions of ethanol (260 °C, 8.0 MPa). Finally, the aerogel was calcined in a muffled furnace at 1200 °C for 5 h in air.

2.2. Catalyst characterization

The surface area and the pore size distribution of the different catalysts were determined by nitrogen adsorption at 77 K on a Micrometrics ASAP 2010 instrument. The surface area was determined according to the Brunauer–Emmett–Teller theory and the analysis of the diameter and the pore volume were carried out according to BJH equation.

The crystal phases of the various catalysts were detected by X-ray diffraction, on a Shimadzu Diffraktometer XD-3A.The operation parameters were: Cu Kα radiation, Ni filter, 30 mA, 40 kV, 2θ scanning from 5 to 80° with the scanning speed of 4° min^{-1}.

The morphologies and sizes of the catalysts were studied using transmission electron microscopy (JEOL, JEM-2000FX) with a voltage of 200 kV. The test samples were prepared by its suspension on the copper net.

Valence state of manganese was monitored by the UV–visible diffuse reflectance spectroscopy using a PE Lambda 35 spectrometer equipped with an integrating sphere. Spectra were recorded at room temperature from 200 to 1100 nm using $BaSO_4$ as reference.

Temperature-programmed desorption of O_2 and temperature-programmed reduction with H_2 were performed using a GC 7890 II gas chromatograph equipped with a TCD. The sample (50 mg) was preheated in flowing air at 800 °C for 1 h before each TPD or TPR test. In TPR analyses a 10 vol.% H_2/Ar mixture (35 cm^3 min^{-1}) was used to reduce the sample by heating 10 °C min^{-1} up to 900 °C. Water produced by the sample reduction was removed by using 5 Å molecular sieve as the desiccant before reaching the detectors. The amount of H_2 uptake in TPR was estimated from the integrated peak areas by comparison with those obtained by using pure CuO as a standard. In O_2 TPD analyses the sample was heated 10 °C min^{-1} up to 900 °C in flowing He (35 cm^3 min^{-1}), meanwhile, the amount of O_2 desorption was calculated by using pure Ag_2O as a standard.

2.3. Activity tests

The reaction of methane combustion was carried out in a conventional flow system under atmospheric pressure. The catalyst (0.8 ml) (20–40 mesh) was loaded in a quartz reactor (i.d. 10 mm), with quartz fiber packed at the end of the catalyst bed. A mixture gas of 4 vol.% O_2 and 1 vol.% CH_4 (nitrogen as balance) was fed into the catalyst bed at GHSV = 15,000 h^{-1}. The inlet and outlet gas compositions were analyzed by an on-line gas chromatography with a packed column of carbon molecular sieve and a thermal conductivity detector.

3. Results and discussion

3.1. Surface area and pore structure

The reaction of catalytic combustion at high temperatures is limited by the mass transfer of reactants to the catalyst surface from the gas phase. Maintaining large surface area and pore structure of combustion catalysts is important in promoting the reaction under the mass transfer limitation [17]. The surface area and pore volume of $Ba_{1-x}La_xMnAl_{11}O_{19-\alpha}$ catalysts are shown in Fig. 1. The $Ba_{1-x}La_xMnAl_{11}O_{19-\alpha}$ catalysts with high surface areas in the range between 45 and 73 m^2/g are obtained. The $Ba_{0.8}La_{0.2}MnAl_{11}O_{19-\alpha}$ catalyst possesses the highest surface area, while the $Ba_{0.4}La_{0.6}MnAl_{11}O_{19-\alpha}$ catalyst possesses the lowest one. The trend of the variation of pore volume is identical to that of surface area, showing the structure of pore plays an important role in determining the surface area

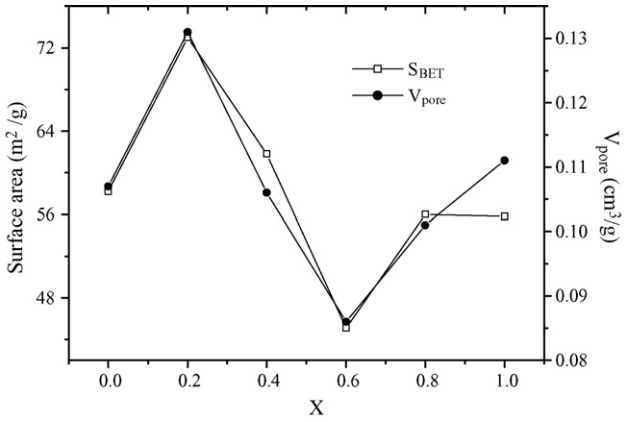

Fig. 1. The surface area and pore volume of the $Ba_{1-x}La_xMnAl_{11}O_{19-\alpha}$ catalysts.

of the catalyst. It is expected that the ion mobility is different due to the introduction of different large cations into the alumina network, which leads to the different capability of maintaining the structure of pore [18]. From the results, it is referred that the $Ba_{0.4}La_{0.6}MnAl_{11}O_{19-\alpha}$ catalyst possesses highest ion mobility at high calcination temperature. Compared with those reported in literature [15], the catalysts in a low pore to crystal size ratio are obtained herein. The possible reason is given as following: since the alumina network forms by using the alumina sol as the co-precipitation precursor before the co-precipitation and the network structure is effectively maintained by using SCD method, the network of the aerogel has a higher stability and more compact structure than that formed by using aluminum nitrate, leading to the decrease in the mobility of aluminum at high temperature. As a result, the growth of crystal is effectively suppressed and the structure of pore is also effectively maintained.

3.2. Crystalline phases

The XRD patterns of the $Ba_{1-x}La_xMnAl_{11}O_{19-\alpha}$ catalysts are shown in Fig. 2. Single hexaaluminate phase is formed when x varies from 0.2 to 1, while α-Al_2O_3 and alumina-rich hexaalu-

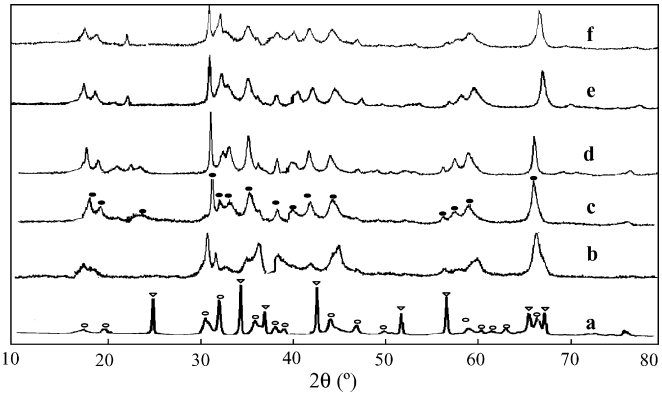

Fig. 2. XRD patterns of the $Ba_{1-x}La_xMnAl_{11}O_{19-\alpha}$ catalysts: (a) x = 0; (b) x = 0.2; (c) x = 0.4; (d) x = 0.6; (e) x = 0.8; (f) x = 1; (●) hexaaluminate; (◯) alumina-rich hexaaluminate; (▽) α-Al_2O_3.

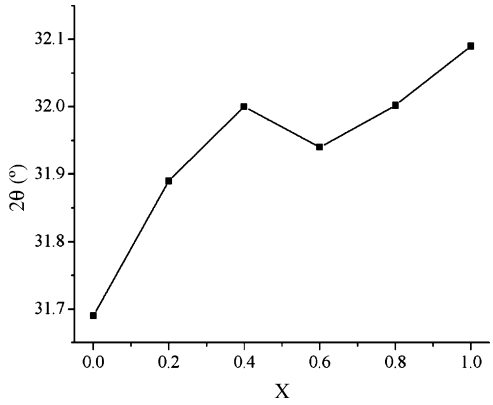

Fig. 3. Effect of x in $Ba_{1-x}La_xMnAl_{11}O_{19-\alpha}$ catalysts on the (1 1 0) diffraction face of β-Al_2O_3 phase.

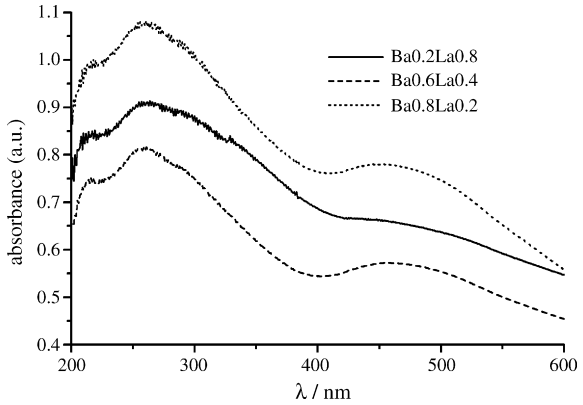

Fig. 5. Diffuse reflectance spectra of the $Ba_{1-x}La_xMnAl_{11}O_{19-\alpha}$ catalysts.

minate ($Ba_{0.717}Al_{11}O_{17.282}$) [JCPDS 83–0270] are observed in the crystalline phases of $BaMnAl_{11}O_{19-\alpha}$ catalyst. The diffraction peaks of Mn oxides could not be observed. That means Mn species were highly dispersed in the hexaaluminate and entered the hexaaluminate lattice. It is obvious that the cation with smaller size and higher valence can promote the formation of hexaaluminate more effectively, probably owing to the more remarkable effect on the charge compensation and the higher ion mobility [8]. The effect of x in $Ba_{1-x}La_xMnAl_{11}O_{19-\alpha}$ catalysts on the (1 1 0) diffraction face of β-Al_2O_3 phase is shown in Fig. 3. The 2θ shifts to a larger angle with the replacement of Ba^{2+} with La^{3+}. The result shows that the magnetoplumbite hexaaluminate tends to form with the replacement of Ba^{2+} with La^{3+} and the property of large cation dominates the type of hexaaluminate [19]. Since the radii of La^{3+} (0.106 nm) cation is smaller than that of Ba^{2+} (0.134 nm), the interval between mirror planes where La^{3+} cations locate is smaller than that of where Ba^{2+} cations locate, which leads to the interval between crystal planes is smaller. Nevertheless, when x is equal to 0.6, The 2θ shifts to a smaller angle probably due to the increase of the distortion of the hexaaluminate lattice. The thermal stability of the hexaaluminate decreases with the increase of the degree of the distortions, which is one factor affecting the surface area of the $Ba_{0.4}La_{0.6}MnAl_{11}O_{19-\alpha}$ catalyst. The catalysts show broad diffraction peaks, indicating they are composed of fine particles. Meanwhile the sizes of the catalysts are different according to the difference of the width of the diffraction peak.

3.3. Microstructure analysis

Fig. 4 presents the TEM results of the catalysts. The catalysts are mainly composed of rod-like particles of 5–20 nm in diameter and 50–150 nm in length. The catalysts with high surface area are obtained due to the small crystalline sizes and the size of the catalyst varies with the modification of the large cations. The result further verifies that the ion mobility is different due to the introduction of different large cations into the alumina network, which is consistent with those from the BET and XRD analysis. Moreover small amount of granular particles are observed in Fig. 2(a), which probably can be assigned to the α-Al_2O_3 crystal. Phase transformation as well as sintering of hexaaluminate tends to begin at neck (or contact) regions that contain abundant vacancies. This model suggests morphology of particles and grain structure will affect the surface area loss rate, i.e. [20]. Rod-like hexaaluminate is effective in retarding sintering because of the small number of contact points between the particles. Hence, the catalysts possess high thermal stability at high temperatures.

3.4. Diffuse reflectance spectroscopy

The $Ba_{1-x}La_xMnAl_{11}O_{19-\alpha}$ catalysts show essentially the identical spectrum that is typical of the MnO_6 chromophore (Fig. 5). Two broad bands at 250 and 450 nm are observed [21]. The 250 nm band is relatively intense, which corresponds to a charge transfer between oxygen anion and manganese cation

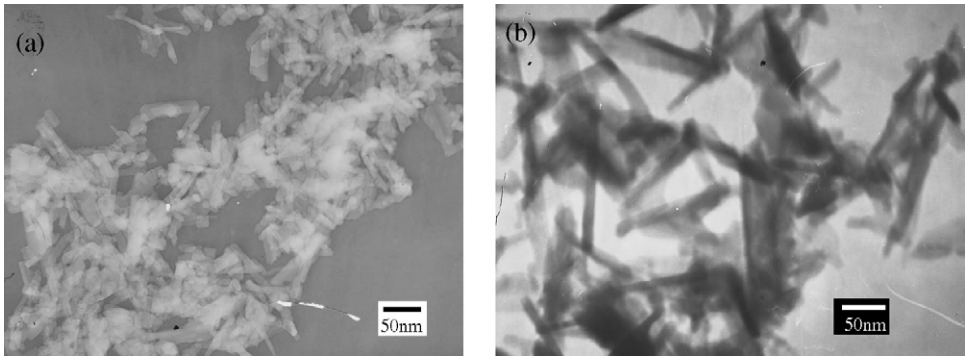

Fig. 4. TEM photographs of the catalysts: (a) $BaMnAl_{11}O_{19-\alpha}$ and (b) $Ba_{0.8}La_{0.2}MnAl_{11}O_{19-\alpha}$.

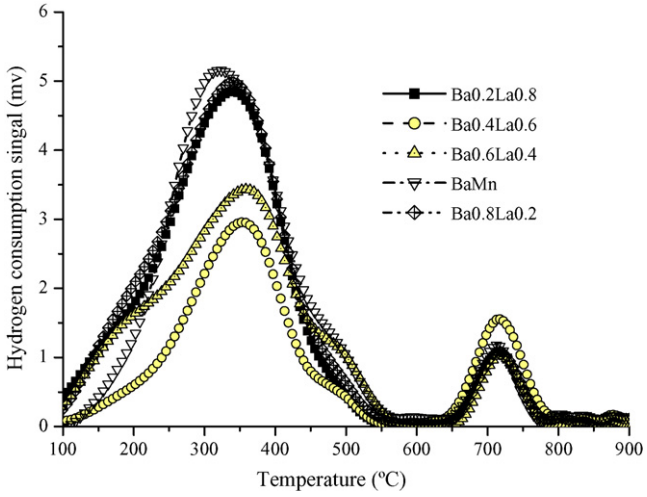

Fig. 6. TPR under hydrogen of the $Ba_{1-x}La_xMnAl_{11}O_{19-\alpha}$ catalysts.

because no d–d transitions are possible at such energies for the first series of transition metal ions. The latter is of lower intensity, which corresponds to the unique spin-allowed d–d transition for a d^4 electronic configuration in an octahedral field. Thus the DRS of the catalysts confirm without ambiguity that manganese does enter the hexaaluminate network and that both symmetry and oxidation state are relevant to Mn^{3+} (Fig. 6).

3.5. TPR measurements

The TPR profiles of the $Ba_{1-x}La_xMnAl_{11}O_{19-\alpha}$ catalysts with two main reduction peaks around 350 and 700 °C are shown in Fig. 4. The former corresponds to the reduction of the Mn^{3+} ions locating in an Al interstitial site near the mirror plane, which are quite easily reduced by hydrogen diffusing quickly between the spinel blocks. While the latter is attributed to the reduction of the Mn^{3+} ions located inside a spinel block, which are more shielded towards reduction. The former is attributed to the most reactive Mn species [22,23]. The difference of reduction temperature shows that the Mn^{3+} ions locate in different distance from the mirror plane, it is inferred that the nature of large cation in mirror plane can affect the thickness of mirror plane, which is identical to the XRD analysis. A minimum temperature is present for $BaMnAl_{11}O_{19-\alpha}$ catalyst, showing the catalyst possesses the thickest mirror plane owing to the largest cations. On the contrary, a maximum one is present for the $Ba_{0.6}La_{0.4}MnAl_{11}O_{19-\alpha}$ catalyst probably due to the distortion of the hexaaluminate lattice. Meanwhile the difference of peak areas reveals that the Mn^{3+} ions with different contents exist in the hexaaluminate lattice. The amounts of total H_2 consumption of $Ba_{1-x}La_xMnAl_{11}O_{19-\alpha}$ catalysts and the mean oxidation state of Mn are given in Table 1.The mean oxidation state of Mn decreases with the replacement of Ba^{2+} with La^{3+} when x varies from 0 to 0.6, which is expectable owing to charge compensation. On the contrary, it increases with the further replacement, probably owing to the easier formation of vacancy and defectiveness on the surface when La^{3+} acts as large cation in the mirror planes in place of Ba^{2+}.

Table 1
Amounts of total H_2 consumption of the $Ba_{1-x}La_xMnAl_{11}O_{19-\alpha}$ catalysts and the mean oxidation state of Mn

Catalysts	H_2 consumption (μmol)	Mean Mn oxidation state
$BaMnAl_{11}O_{19-\alpha}$	5.73	2.182
$Ba_{0.8}La_{0.2}MnAl_{11}O_{19-\alpha}$	5.67	2.180
$Ba_{0.6}La_{0.4}MnAl_{11}O_{19-\alpha}$	4.58	2.145
$Ba_{0.4}La_{0.6}MnAl_{11}O_{19-\alpha}$	4.20	2.133
$Ba_{0.2}La_{0.8}MnAl_{11}O_{19-\alpha}$	5.41	2.172

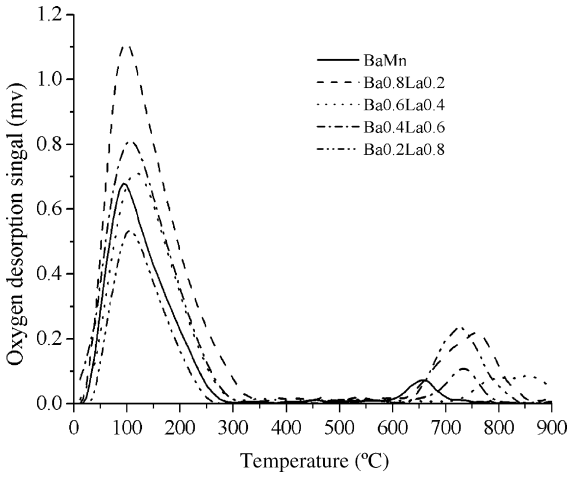

Fig. 7. TPD profiles of oxygen from the $Ba_{1-x}La_xMnAl_{11}O_{19-\alpha}$ catalysts.

3.6. O_2-TPD

TPD profiles of oxygen from the $Ba_{1-x}La_xMnAl_{11}O_{19-\alpha}$ catalysts with two main desorption peaks around 150 and 750 °C are shown in Fig. 7. The first one, probably, corresponds to the physically adsorbed oxygen on the catalyst surface, while the latter to the lattice oxygen, which probably corresponds to the oxygen anions loosely locating in the hexaaluminate lattice rather than ones closely locating inside a spinel block due to uneasy desorption. The temperature and the amount of lattice oxygen desorption from $Ba_{1-x}La_xMnAl_{11}O_{19-\alpha}$ catalysts are given in Table 2. The difference of the temperature shows that the oxygen anions on the mirror plane possess different mobility, which affects the activity of lattice oxygen. The lowest temperature (656 °C) is present for the $BaMnAl_{11}O_{19-\alpha}$ catalyst and the highest (826 °C) for the $Ba_{0.4}La_{0.6}MnAl_{11}O_{19-\alpha}$ catalyst. The result reveals that the $BaMnAl_{11}O_{19-\alpha}$ catalyst possesses the

Table 2
the temperature and the amount of lattice oxygen desorption from the $Ba_{1-x}La_xMnAl_{11}O_{19-\alpha}$ catalysts

Catalysts	Desorption temperature (°C)	Oxygen desorption (μmol/g)
$BaMnAl_{11}O_{19-\alpha}$	656	8.48
$Ba_{0.8}La_{0.2}MnAl_{11}O_{19-\alpha}$	759	52.6
$Ba_{0.6}La_{0.4}MnAl_{11}O_{19-\alpha}$	826	26.2
$Ba_{0.4}La_{0.6}MnAl_{11}O_{19-\alpha}$	735	25
$Ba_{0.2}La_{0.8}MnAl_{11}O_{19-\alpha}$	725	53

Table 3
Catalytic activity expressed as $T_{10\%}$, $T_{50\%}$ and $T_{90\%}$ in °C and as intrinsic activity (10^{-5} mol CH_4 converted per hour and per square meter)

Catalyst	$T_{10\%}$ (°C)	$T_{50\%}$ (°C)	$T_{90\%}$ (°C)	Intrinsic activity at 500 °C
$BaMnAl_{11}O_{19-\alpha}$	470	576	651	7.6
$Ba_{0.8}La_{0.2}MnAl_{11}O_{19-\alpha}$	462	577	647	7.6
$Ba_{0.6}La_{0.4}MnAl_{11}O_{19-\alpha}$	554	641	720	1.9
$Ba_{0.4}La_{0.6}MnAl_{11}O_{19-\alpha}$	480	604	688	7.7
$Ba_{0.2}La_{0.8}MnAl_{11}O_{19-\alpha}$	458	560	642	8.7
$LaMnAl_{11}O_{19-\alpha}$	565	690	820	1.8

most active lattice oxygen. It is expected that the oxygen anions located most loosely on the thickest mirror plane. The result is also confirmed by the H_2-TPR analysis. Meanwhile the difference of peak areas reveals that the catalysts possess the lattice oxygen with different contents. The $BaMnAl_{11}O_{19-\alpha}$ catalyst possesses the lowest content of lattice oxygen, which indicating the content of lattice oxygen increases with the introduction of La^{3+}. Meanwhile the $Ba_{0.2}La_{0.8}MnAl_{11}O_{19-\alpha}$ catalyst possesses the highest content.

3.7. Catalytic activity of methane combustion

$T_{10\%}$, $T_{50\%}$ and $T_{90\%}$ corresponding to 10, 50 and 90% conversion are respectively reported in Table 3. The catalysts with high catalytic activities are obtained except for the $LaMnAl_{11}O_{19-\alpha}$ catalyst. The lowest ignition temperature ($T_{10\%}$) and the lowest complete conversion of methane temperature ($T_{90\%}$) are obtained at $x = 0.8$, indicating that the $Ba_{0.2}La_{0.8}MnAl_{11}O_{19-\alpha}$ catalyst possesses the highest catalytic activity owing to the highest content of lattice oxygen. Meanwhile, the $Ba_{0.8}La_{0.2}MnAl_{11}O_{19-\alpha}$ catalyst possesses the high catalytic activity and thermal stability owing to the highest surface area. Moreover, the $BaMnAl_{11}O_{19-\alpha}$ catalyst possesses the high catalytic activity owing to the most active lattice oxygen. On the contrary, the $Ba_{0.6}La_{0.4}MnAl_{11}O_{19-\alpha}$ catalyst possesses the lowest catalytic activity due to the lowest ability of activating oxygen. From above, we conclude that the lattice oxygen plays an important role in the catalytic reaction. The intrinsic activities of the $Ba_{1-x}La_xMnAl_{11}O_{19-\alpha}$ catalysts are also given in Table 3. The maximum value is obtained at $x = 0.8$.

4. Conclusions

Mn-Substituted Ba-La-hexaaluminate rod-like nanoparticles with high surface area in the range between 45 and 73 m^2/g have been prepared using the alumina sol as the $(NH_4)_2CO_3$ co-precipitation precursor and the supercritical drying method. The properties and microstructures of the catalysts are determined by the ion mobility at high calcination temperature. Since the alumina network formed by using the alumina sol as the co-precipitation precursor has a higher stability and more compact structure than that formed by using aluminum nitrate, leading to the decrease in the mobility of aluminum at high temperature. Hence the catalysts obtained herein are different from those reported previously. The nature of the large cation in the mirror plane can affect the Mn^{2+}/Mn^{3+} redox process. The $Ba_{0.2}La_{0.8}MnAl_{11}O_{19-\alpha}$ catalyst possesses the highest catalytic activity owing to the excellent performance of activating oxygen.

References

[1] L.D. Pfefferle, W.C. Pfefferle, Catal. Rev. Sci. Eng. 29 (1987) 219.
[2] M.F.M. Zwinkels, S.G. Järås, P.G. Menon, Catal. Rev. Sci. Eng. 35 (1993) 319.
[3] M. Machida, A. Sato, T. Kijima, H. Inoue, K. Eguchi, H. Arai, Catal. Today 26 (1995) 239.
[4] K. Eguchi, H. Arai, Catal. Today 29 (1996) 379.
[5] M. Machida, K. Eguchi, H. Arai, J. Catal. 123 (1990) 477.
[6] H. Inoue, K. Sekizawa, K. Eguchi, H. Arai, J. Solid State Chem. 121 (1996) 190.
[7] Ben W.-L. Jang, R.M. Nelson, J.J. Spivey, M. Ocal, R. Oukaci, G. Marcelin, Catal. Today 47 (1999) 103.
[8] G. Groppi, C. Cristiani, P. Forzatti, Appl. Catal. B 35 (2001) 137.
[9] Debra R. Rolison, Science 299 (2003) 1698.
[10] A.J. Zarur, J.Y. Ying, Nature 403 (2000) 65.
[11] A.J. Zarur, H.H. Hwu, J.Y. Ying, Langmuir 16 (2000) 3042.
[12] P.K. Sahu, B.D. Kulkarni, R.B. Khomane, S.A. Pardhy, U.D. Phalgune, P. Rajmohanan, R. Pasricha, Chem. Comm. 15 (2003) 1876.
[13] F. Teng, J. Xu, Z. Tian, J. Wang, Y. Xu, Z. Xu, G. Xiong, L. Lin, Chem. Comm. 15 (2004) 1858.
[14] S.J. Cho, Y.S. Seo, K.S. Song, N.J. Jeong, S.K. Kang, Appl. Catal. B 30 (2001) 351.
[15] J. Wang, Z. Tian, J. Xu, Y. Xu, Z. Xu, L. Lin, Catal. Today 83 (2003) 213.
[16] G. Groppi, M. Bellotto, C. Cristiani, P. Forzatti, P.L. Villa, Appl. Catal. A 104 (1993) 101.
[17] M. Machida, K. Eguchi, H. Arai, J. Catal. 103 (1987) 385.
[18] T.-F. Yeh, H.-G. Lee, K.-S. Chu, C.-B. Wang, Mater. Sci. Eng. A 384 (2004) 324.
[19] G. Groppi, F. Assandri, J. Solid State Chem. 114 (1995) 326.
[20] H. Arai, M. Machida, Appl. Catal. A 138 (1996) 161.
[21] P. Artizzu-Duart, J.M. Millet, N. Guilhaume, E. Garbowski, M. Primet, Catal. Today 59 (2000) 163.
[22] P. Artizzu-Duart, Y. Brullé, F. Gaillard, E. Garbowski, N. Guilhaume, M. Primet, Catal. Today 54 (1999) 181.
[23] M. Astier, E. Garbowski, M. Primet, Catal. Lett. 95 (2004) 31.